Membrane Lipids Augment Cell Envelope Stress Signaling and Resistance to Antibiotics and Antimicrobial Peptides in *Enterococcus faecalis*

William R Miller[1,2,3], April Nguyen [1,2,4,5], Kavindra V Singh[1,2], Samie Rizvi[1,2], Ayesha Khan[4,5,#], Sam G Erickson[4], Stephanie L Egge[1,2], Melissa Cruz[4,5], An Q Dinh[1,2], Lorena Diaz[7], Rutan Zhang[8], Libin Xu[8], Danielle A Garsin[4,5], Yousif Shamoo[9], Cesar A Arias[1,2,3,6]

1. Division of Infectious Diseases, Houston Methodist Hospital, Houston, Texas, USA

2. Center for Infectious Diseases, Houston Methodist Research Institute, Houston, Texas, USA

3. Department of Medicine, Weill Cornell Medical College, New York, New York, USA

4. McGovern Medical School, University of Texas Health Science Center, Houston, TX, USA

5. Microbiology and Molecular Genetics, Graduate School of Biomedical Sciences, University of Texas Health Science Center, Houston, TX, USA

6. Molecular Genetics and Antimicrobial Resistance Unit, Universidad El Bosque, Bogota, Colombia

7. Genomics and Resistant Microbes Group, Facultad de Medicina Clinica Alemana, Universidad del Desarrollo and Millennium Initiative for Collaborative Research On Bacterial Resistance (MICROB-R), Santiago, Chile

8. Department of Medicinal Chemistry, University of Washington, Seattle, Washington, USA.

9. Department of Biosciences, Rice University, Houston, TX, USA

Corresponding Author: William Miller, Division of Infectious Diseases, Houston Methodist Hospital, 6560 Fannin St, Scurlock Tower Suite 1540, Houston, TX 77030

Email: wrmiller@houstonmethodist.org

#Current Address: Department of Pathology, Microbiology, and Immunology, Vanderbilt University Medical Center, 1211 Medical Center Drive, Nashville, TN 37232.

Abstract

Enterococci have evolved resistance mechanisms to protect their cell envelopes against bacteriocins and host cationic antimicrobial peptides (CAMPs) produced in the gastrointestinal environment. Activation of the membrane stress response has also been tied to resistance to the lipopeptide antibiotic daptomycin. However, the actual effectors mediating resistance have not been elucidated. Here, we show that the MadRS (formerly YxdJK) membrane antimicrobial peptide defense system controls a network of genes, including a previously uncharacterized three gene operon (*madEFG*) that protects the *E. faecalis* cell envelope from antimicrobial peptides. Constitutive activation of the system confers protection against CAMPs and daptomycin in the absence of a functional LiaFSR system and leads to persistence of cardiac microlesions *in vivo*. Moreover, changes in the lipid cell membrane environment alter CAMP susceptibility and expression of the MadRS system. Thus, we provide a framework supporting a multilayered envelope defense mechanism for resistance and survival coupled to virulence.

54 Enterococci are a leading cause of healthcare-associated infections and possess a
55 diverse array of intrinsic and acquired antimicrobial resistance determinants.[1,2] These organisms
56 are commensal colonizers of the gastrointestinal tract, where they are exposed to cationic
57 antimicrobial peptides (CAMPs) produced by the innate immune system.[3] Several important
58 antibiotics used in clinical practice, including the lipopeptide daptomycin, share functional
59 similarities with CAMPs.[4] Daptomycin possesses a peptide core with an acyl tail, and in
60 conjunction with calcium forms an amphipathic complex that binds the membrane lipid
61 phosphatidylglycerol (PG) and the undecaprenyl intermediates of cell wall synthesis.[5]
62 Daptomycin binding displaces enzymes necessary for cell envelope genesis, ultimately leading
63 to membrane disruption and bacterial cell death. The widespread frequency of multidrug
64 resistance in both *Enterococcus faecium* and *E. faecalis* has led to a reliance on daptomycin for
65 treatment of recalcitrant invasive vancomycin-resistant enterococcal (VRE) infections.

66 As members of the gastrointestinal flora, enterococci have evolved several mechanisms
67 to sense and respond to CAMPs. This survival strategy involves activation of cell stress
68 response signaling systems in conjunction with changes in the synthesis of cell membrane
69 phospholipids.[6-9] In particular, the LiaFSR system of *E. faecalis* has been linked to survival in
70 the presence of daptomycin, the cathelicidin LL-37, and other CAMPs, via a secreted protein
71 (LiaX), which plays a dual sensing and regulatory role mediated by the N- and C-terminal
72 domains, respectively.[10] While substitutions in the LiaFSR system lead to antibiotic tolerance, or
73 loss of bactericidal daptomycin activity, additional changes in enzymes related to membrane
74 lipid biosynthesis are required for the full resistance phenotype. Since the LiaFSR pathway is
75 also a major mediator of daptomycin resistance in clinical settings, the selective pressure
76 exerted by CAMPs has important therapeutic repercussions.

77 Experimental evolution in the presence of daptomycin using both *E. faecalis* and *E.*
78 *faecium* strains lacking the LiaR response regulator and, therefore, deficient in LiaFSR
79 signaling, suggested that activation of the YxdJK two-component system in the presence of
80 mutations in *dak* (encoding a putative fatty acid kinase) could also lead to the development of
81 daptomycin resistance.[7,11] The YxdJK system shares homology with other ABC transporters
82 involved in lantibiotic and antimicrobial peptide resistance, including the BceRS-BceAB system
83 from *Bacillus subtilis* and the GraRS-VraDE system from *Staphylococcus aureus*, although it
84 falls in a distinct group apart from these two systems based on phylogenetic analysis.[12] Dak is a
85 homologue of the fatty acid kinase Fak in *S. aureus*, responsible for the first step in
86 incorporation of exogenous fatty acids into bacterial phospholipids.[13] Of note, fatty acids have

been implicated in increasing survival in the presence of daptomycin and other membrane stressors.[14] As the specific mechanism by which *E. faecalis* defends the cell envelope against CAMPs is unknown, we sought to determine the role of *dak* and the YxdJK system (which we hereafter refer to as the MadRS system for membrane antimicrobial peptide defense), in cell envelope protection against daptomycin and host-derived CAMPs.

Results

Identification of the MadRS regulon. We previously described an alanine to aspartate substitution at amino acid position 202 in the MadS histidine kinase associated with daptomycin resistance in *E. faecalis*.[7] To investigate the functional importance of this change, we introduced this allele into *E. faecalis* OG1RF (OG1RF$madS_{A202E}$). The presence of $madS_{A202E}$ was sufficient to increase the minimum inhibitory concentration (MIC) of daptomycin from 1.5 to 6 µg/mL, and the MIC of bacitracin from 32 to 96 µg/mL (**Table 1**). In the OG117 background (a derivative of OG1RF adapted for CRISPR based manipulation), introduction of both the $madS_{A202E}$ allele and deletion of the *dak* gene, led to an increase in daptomycin and bacitracin MICs (**Table 1**). Although the MadRS system is known to mediate protection from the antibiotic bacitracin via the presence of the ABC transporter MadLM (previously YxdLM), we hypothesized that this transporter may also be involved in the daptomycin resistance phenotype, similar to VraDE in *S. aureus*.[15,16] However, deletion of the genes encoding MadLM from the chromosome of the daptomycin resistant *E. faecalis* OG117Δ*dak*$madS_{A202E}$ led to a decrease in the MIC of bacitracin, but did not alter susceptibility to daptomycin (**Table 1**). Thus, we applied a transcriptomic approach to identify additional genes under control of the MadRS system that could explain the changes in daptomycin MIC.

We compared differentially expressed genes in OG1RFΔ*madR*, which lacks the response regulator of the MadRS system, and OG1RF$madS_{A202E}$ to the parent strain OG1RF in the presence and absence of daptomycin (**Figure 1A-B**, **Table S1**). Comparing OG1RFΔ*madR* to OG1RF, there were 8 genes with a significant difference in expression in the absence of daptomycin exposure. The most strongly downregulated was a previously unidentified putative operon of three genes, *madEFG*, followed by *madLM*, as well as the genes *mprF2* (which catalyzes the production of lysyl-PG) and *salA* (a peptidoglycan hydrolase, **Table S1**). In OG1RF$madS_{A202E}$, there were 364 and 368 differentially expressed genes in the absence and presence of daptomycin, respectively. The most significant changes included increased

119 expression of the *madEFG* operon, the *dlt* operon (involved in D-alanylation of lipoteichoic
120 acids), *madLM*, *salA*, and downregulation of the *upp* gene, annotated as a uracil
121 phosphoribosyltransferase. To confirm these results, we performed qRT-PCR for the genes
122 *madG*, *madL*, *dltA*, and *madA*, which was previously identified as a component of the MadRS
123 signaling network with minimal differences in expression under bacitracin induction. In the *madR*
124 knockout, a decrease in gene expression for *madG* and *madL* was identified as compared to
125 OG1RF both in the presence and absence of daptomycin. There was no significant difference in
126 expression of either *madA* or *dltA*. In the $madS_{A202E}$ background, there was a significant
127 increase in the expression of *madG*, *madL*, and *dltA*, particularly on exposure to daptomycin
128 (**Figure 1C**).

129 **The MadRS network provides a targeted response to antibiotics and host derived AMPs.**
130 To study the effects of each component of the MadRS system, we constructed a series of
131 deletion mutants targeting *madLM*, *madEFG* and *dltA* in daptomycin-resistant
132 OG117Δ$dakmadS_{A202E}$. Deletion of *madLM* or *madEFG* had no impact on the MIC of
133 daptomycin, while deletion of both led to a modest decrease (12 to 8 µg/mL; **Table 1**). In
134 contrast, deletion of *dltA* resulted in a reduction of 8-fold in the in daptomycin MIC (12 to 1.5
135 µg/mL), similar to wild type OG117. Since *madEFG* did not appear to alter susceptibility to either
136 bacitracin or daptomycin but were among the most significantly expressed genes under the
137 control of MadR, we investigated alternative roles for MadEFG.

138 Given the similarities between daptomycin and CAMPs, we assayed the activity of
139 several representative CAMPs, including LL-37 (cathelicidin), human β-defensin 3 (HBD3), and
140 human neutrophil peptide-1 (HNP1, α-defensin) against the MadRS knockout mutants (**Figure**
141 **2A-B, Supplemental Figure 1**). In the presence of LL-37 at 50 µg/mL, there was a significant
142 increase in survival of OG117Δ$dakmadS_{A202E}$ versus OG117 (mean difference 42.6%,
143 p=0.0001). Deletion of *madEFG*, but not *madLM* or *dltA*, resulted in a reversion of the survival
144 benefit (mean difference from OG117 1.79%, p=0.99), and complementation with *madEFG* at
145 the native chromosomal location restored bacterial survival (mean difference 36%, p=0.0001).
146 For HBD3, deletion of *dak* was sufficient to increase survival (mean difference 47.4%,
147 p=0.0003), comparable to the survival of the OG117Δ$dakmadS_{A202E}$ mutant. Restoring the *dak*
148 gene in the native chromosomal location restored HBD3 activity to wild type levels (mean
149 difference 12.2%, p=0.72). Loss of *madEFG* resulted in a decrease in HBD3 survival by 10.1%,
150 but this was not statistically significant. Interestingly, no change in survival was seen for any
151 strain with the α-defensin HNP1 (**Supplemental Figure 1)**.

152 **MadRS mediates survival in the presence of CAMPs independent of LiaFSR.** The LiaFSR
153 system has been implicated as the major mediator of cell envelope homeostasis under
154 daptomycin stress in enterococci. Furthermore, the addition of exogenous N-terminal LiaX has
155 been shown to activate LiaFSR signaling and provide protection against membrane stress even
156 in daptomycin-sensitive *E. faecalis* isolates.[10] Thus, we sought to characterize the distinct roles
157 of MadRS compared to LiaFSR in the cell envelope stress response. Introduction of the
158 $madS_{A202E}$ allele into OG1RFΔ*liaR* (lacking activation of LiaFSR due to deletion of the gene
159 encoding the response regulator) was sufficient to increase survival in the presence of LL-37
160 (mean difference 41.4%, p<0.0001, **Figure 2C**), suggesting that a functional LiaFSR response
161 was not necessary for MadRS mediated protection against LL-37. Conversely, deletion of the
162 gene encoding the MadR response regulator in OG1RF resulted in decreased survival in the
163 presence of LL-37 (3.8% versus 11.8%), an effect that could not be rescued with the addition of
164 exogenous LiaX, despite the strain retaining a functional LiaFSR system. A similar pattern was
165 seen with daptomycin, with decreased survival in the *madR* deletion strain that could not be
166 rescued by addition of LiaX (**Figure 2D**). These findings indicated that MadRS ultimately
167 controls the effector systems responsible for CAMP resistance in *E. faecalis*.

168 To test this hypothesis, we made targeted deletions of the genes encoding MadEFG and
169 DltA in the OG117Δ*liaX* background, where the LiaFSR system is constitutively expressed due
170 to loss of the regulatory C-terminal domain of LiaX. Consistent with previous results, the
171 OG117Δ*liaX* strain showed enhanced survival in the presence of LL-37 as compared to OG117
172 (71.5% vs 8.31%, p=0.0001, **Figure 2E**). Deletion of *madEFG* in this background led to a
173 decrease in survival (71.5% vs 33.7%, p=0.013), suggesting this system plays a significant role
174 in membrane defense against LL-37, even in the presence of a constitutively active LiaFSR
175 response. The loss of *dltA* led to a 27.9% reduction in survival after exposure to LL-37 in the
176 OG117Δ*liaX* background that was not statistically significant. Interestingly, in the OG117Δ*liaX*
177 background loss of *madEFG* led to a significant decrease in survival in the presence of HBD3
178 (70.9% vs 36.4%, p=0.013, **Figure 2F**), suggesting that the MadRS system can respond to
179 CAMPs such as β-defensins and cathelicidins.

180 MadEFG did not appear to directly impact daptomycin susceptibility; however, a
181 reduction in the MIC of daptomycin from 12 to 2 μg/mL was observed in the OG117Δ*liaX*Δ*dltA*
182 strain, and the MIC was restored on complementation of *dltA* in the native chromosomal
183 location. Since D-alanylation of teichoic acids has been implicated in changes of cell surface
184 charge and daptomycin resistance in *S. aureus*, we evaluated cell surface charge using a

185 cytochrome c binding assay (**Supplemental Figure 2**). As compared to OG117, OG117Δ*liaX*
186 displayed a small but significant increase in positive cell surface charge. This increase was
187 abolished in the OG117Δ*liaX*Δ*dltA* strain and restored on complementation of *dltA*. In the
188 OG117Δ*dak* background, there was a small increase in cell surface charge of the *dak* deletion
189 mutant, but no significant changes across any of the other strains. Thus, a simple electrostatic
190 repulsion model cannot sufficiently explain the phenotypic changes observed in *E. faecalis*.

191 **Loss of *dak* alters the membrane lipid environment and leads to activation of MadRS in**
192 **the absence of antibiotic stress.** We have previously shown that *E. faecalis* with a truncated
193 C-terminal Dak deletion have a growth defect and more rigid cell membrane.[7] The *dak* gene is
194 predicted to encode a fatty acid kinase which, in *S. aureus*, has been shown to mediate
195 phosphorylation of exogenous fatty acids for use in membrane biosynthesis.[13] In the absence of
196 *dak*, the endogenous type II fatty acid synthesis pathway (FASII) supplies acyl-chains for
197 phospholipid synthesis. Consistent with this hypothesis, OG117Δ*dak* has increased sensitivity
198 to triclosan (4 µg/mL), an inhibitor of the FabI enoyl-ACP reductase of FASII, as compared to
199 wild type OG117 or the *dak* complemented strain (both 16 µg/mL). During construction of the
200 OG117Δ*dak* derivatives, we noted that OG117Δ*dakmadS*$_{A202E}$ and subsequent strains had a
201 restoration of growth (**Supplemental figure 3**). Whole genome sequencing of these strains
202 showed a serine to tyrosine change at amino acid 36 of FabT, a MarR transcriptional repressor
203 which binds upstream of the Fab operon (encoding the FASII enzymes). Based on alignment
204 with FabT from *Streptococcus pneumoniae*, for which the crystal structure has been solved, this
205 change would be predicted to fall in the DNA binding domain, potentially impairing the binding of
206 the repressor and, thus, resulting in constitutive expression of the Fab operon.[17] Colonies with
207 the mutations in FabT had no change in triclosan susceptibility compared to OG117Δ*dak* (4
208 µg/mL), consistent with continued reliance on endogenous FA synthesis.

209 To assess the membrane changes associated with the absence of *dak*, we performed
210 hydrophilic interaction chromatography-mass spectrometry (HILIC-MS) to characterize the
211 phospholipids of OG117, OG117Δ*dak*, and the OG117Δ*dak*::*dak* complemented strain, as well
212 as OG117Δ*dakmadS*$_{A202E}$ (**Figure 3A and 3B**) during exponential growth and stationary phase.
213 In exponential phase, OG117Δ*dak* had a significant decrease in the abundance of PG, Lysyl-
214 PG (LPG), and diacyglycerol (DG) as compared to OG117. In both the *dak* complemented and
215 the OG117Δ*dakmadS*$_{A202E}$ strain (with the mutation in *fabT*), there were no significant changes
216 in phospholipid abundance. In stationary phase, the OG117Δ*dakmadS*$_{A202E}$ strain had a
217 significantly higher abundance of PG and LPG as compared to OG117, consistent with the

218 increased expression of *mprF2* (the product of which synthesizes LPG) in the *madS*$_{A202E}$ mutant.
219 The acyl chain composition of each lipid species in exponential and stationary phase is shown
220 in **Figure 3C** and **Supplemental Table 2**. Strains with a deletion of *dak* showed a relative
221 increase in shorter chain and saturated fatty acids as compared to OG117 during exponential
222 phase growth.

223 To investigate whether the altered membrane environment associated with the deletion
224 of *dak* influenced expression of the wild type MadRS system, we evaluated the expression of
225 *madG* with and without antibiotic stress in the *dak* mutant strains during exponential growth
226 (**Figure 3D**). In the absence of antibiotic stress, there was a 2-fold increase in the expression of
227 *madG* in the *dak* deletion mutant as compared to OG1RF, similar to the 2-fold induction of
228 *madG* expression seen after exposure to daptomycin in all strains. Bacitracin led to a robust
229 expression of *madG* that did not differ across strains. Taken together, our results suggest that
230 changes in phospholipid composition due to the deletion of *dak* both directly contribute to CAMP
231 resistance and prime the transcriptional response of the MadRS system.

232 **MadRS is associated with CAMP dependent changes in survival of *Caenorhabditis***
233 ***elegans*.** Using a *C. elegans* infection model, we examined the role of the MadRS system in
234 protecting enterococci from CAMPs produced by the innate immune system. In wild type *C.*
235 *elegans*, there was an attenuation of the OG1RFΔ*madR* strain as compared to OG1RF (median
236 survival 11 days versus 6 days, $p<0.0001$, **Figure 4A**). This phenotype was reversed with
237 complementation of *madR* on a plasmid with minimal differences between OG1RF and the
238 complemented strain (median survival 6 versus 7 days, $p=0.01$). To examine if this survival
239 difference was influenced by the presence of host CAMPs, we performed the same survival
240 assay in *C. elegans* lacking the *pmk-1* gene, which encodes an ortholog of the p38 MAP kinase
241 necessary for production of CAMPs. **Figure 4B** shows that there were no differences in survival
242 between Δ*pmk-1* worms infected with OG1RF, OG1RFΔ*madR*, or the complemented strain,
243 supporting the notion that the presence of CAMPs mediates survival of *C. elegans* infected with
244 *E. faecalis* lacking MadR, rather than a general change in strain virulence.

245 **The *madS*$_{A202E}$ allele is associated with an increased burden of cardiac microlesions in a**
246 **mouse peritonitis model of infection.** Given the importance of host CAMPs to the innate
247 immune response, we sought to investigate the *in vivo* impact of the MadRS system in a mouse
248 model of peritonitis. We examined overall survival, bacterial burden in the spleen, and the
249 average number and size of cardiac microlesions as assessed by histopathology of cardiac
250 tissue from infected mice.[18] There was no difference in median survival or bacterial burden in

251 the spleen between OG1RF, OG1RFΔ*madR*, and OG1RF*madS*$_{A202E}$ (**Supplemental Figure 5**).
252 However, mice infected with OG1RF*madS*$_{A202E}$ showed an increase in the mean number of
253 cardiac microlesions per histopathological section as compared to OG1RFΔ*madR* (1.48 vs. 0.1,
254 p=0.009, **Figure 4C-G**), and a significantly larger lesion area as compared to OG1RF (p<0.001).
255 The findings suggest that the MadRS system may play a critical role in the immune mediated
256 clearance of deep seated cardiac enterococcal infections.

257

258 **Discussion**

259 The potential for cross resistance between daptomycin and CAMPs of the innate
260 immune system is of particular concern, since enterococcal exposure to CAMP in the GI tract
261 has the potential to prime antibiotic resistance and serve as a precursor to mucosal
262 translocation and bloodstream infections, particularly in the immunocompromised host.[19-21] In
263 this study, we characterized a specific defense network that protects the enterococcal cell
264 envelope and dissected the effector genes responsible for resistance to CAMPs and peptide-
265 like antibiotics.

266 Using transcriptional analyses, we identified the regulatory network of the MadRS
267 system, showing that it has a much broader cell envelope protective effect than previously
268 known (**Figure 5**). Consistent with prior results, MadR was responsible for the expression of
269 MadLM and that activation of the system also resulted in an increase in the expression of the *dlt*
270 operon.[22] In addition, MadR appears to regulate the expression of the peptidoglycan hydrolase
271 SalA, the lysylphosphatidylglycerol synthetase MprF2, and the novel *madEFG* operon, which
272 had not been previously characterized in *E. faecalis*. The *madEFG* genes share sequence
273 identity with the *spr0693-0695* operon in *Streptococcus pneumoniae*, which has been shown to
274 encode a MacAB-like efflux pump with LL-37 as a potential substrate.[23] The product of *spr0693*
275 was predicted to form a hexameric channel of ~155 Å, potentially spanning the peptidoglycan
276 layer. Thus, we postulate that MadEFG is likely to function by removing CAMPs at the
277 membrane interface and transporting them past the peptidoglycan layer. The other components
278 of the MadRS regulon alter the cell envelope by D-alanylation of wall teichoic acids via Dlt or
279 production of lysyl-phosphatidylglycerol via MprF to prevent diffusion of CAMPs back to the
280 membrane surface. Interestingly, no obvious homologues of *madEFG* are present in the
281 genome of *Enterococcus faecium* DO, suggesting that there are important differences in the
282 mechanism underlying membrane defense between the two species.

283 Alterations of the membrane bilayer, as we observed in the *dak* knockout, may provide a
284 further barrier to effective CAMP action. Loss of Dak function resulted in a membrane lipid fatty
285 acid profile that contained significantly more saturated fatty acids, in part explaining our prior
286 observation of decreased membrane fluidity (presumably from a tighter lipid packing order) in
287 the Dak mutant.[7] These changes were sufficient to decrease the activity of HBD3, and also
288 appear to prime the MadRS system by leading to an increase in the baseline transcription of
289 target genes, thus, preparing the cell to defend against CAMPs. Thus, the membrane lipid
290 environment has both a direct and indirect role in antimicrobial resistance, and these findings
291 may explain why mutations in both phospholipid metabolism and cell envelope stress response
292 networks emerge together in daptomycin-resistant isolates.

293 Importantly, the MadRS response appears to complement the global stress response of
294 LiaFSR with a targeted set of effector proteins. Recently, a link between the LiaFSR and
295 MadRS systems was demonstrated in *E. faecalis*, with activation of the LiaFSR system
296 associated with increased expression of MadRS.[24] Similar to the Bce-type transporters, MadAB-
297 MadS are likely to function via a flux-sensing mechanism, where the transport activity of MadAB
298 is coupled to the kinase activity of MadS.[25] The data presented here suggest that the
299 emergence of daptomycin resistance via MadRS arises via a decoupling of the MadS kinase
300 and the MadAB flux sensor, as the $MadS_{A202E}$ mutant showed increased expression of the
301 genes of the MadR regulon, even in the absence of antibiotic stress. This decoupling bypassed
302 the potential transcriptional regulation of the MadRS system by LiaFSR, and activation of
303 MadRS results in a survival advantage against CAMPs, even in the absence of *liaR*.

304 Moreover, the results from the *C. elegans* and mouse peritonitis models suggest that the
305 MadRS system also plays a major role against CAMPs *in vivo*, and resistance arising via this
306 pathway may have implications for the clearance of deep-seated infections such as infective
307 endocarditis. Interestingly, we did not see a difference in bacterial burden in the spleen. One
308 possibility is that immune mediated clearance via macrophages and neutrophils may be
309 preserved via activity of alternate peptides such as HNP-1, the activity of which was not affected
310 in our assay conditions. Since peptides such as β-defensins and cathelicidins are an important
311 part of mucosal barrier defense, this resistance pattern may predispose to invasive infection and
312 bacteremia, particularly in immunocompromised hosts with neutropenia.[26,27] Further work is
313 needed to understand the role of this system with respect to colonization of the GI tract and
314 subsequent risk for translocation and infection.

In summary, the MadRS system controls a network of genes in *E. faecalis* that are capable of conferring resistance to the antibiotic daptomycin and host immune peptides including HBD3 and LL-37. In *E. faecalis*, survival in the presence of these CAMPs is dependent on the presence of *madEFG*, a three gene operon predicted to encode a MacAB-like efflux pump, with alterations in membrane lipids also contributing to HBD3 resistance. Mutations leading to constitutive activation of the MadRS system are able to provide daptomycin resistance independent of LiaFSR, and our *in vivo* data suggest this system may play an important role in the persistence of enterococcal infections.

Acknowledgements

The authors wish to thank Rafael Rios for assistance with the RNA-Seq analysis. WRM is supported by a National Institute of Health, Institute of Allergy and Infectious Diseases (NIH/NIAID) grant K08 AI135093. CAA is supported by a NIH/NIAID K24 AI121296, R01 AI148342, R01 AI134637, and P01 AI152999. DAG is supported by R01 DE027608, R01 AI150045, and R21 AI167124. SLE was supported by a training fellowship from the Gulf Coast Consortia, Texas Medical Center Training Program in Antimicrobial Resistance (TPAMR) (NIAID) T32 AI141349. YS is supported by NIAID R01 A1080714. LX is supported by NIH/NIAID R01 AI136979.

Conflict of Interest

WRM has received grant support from Merck and royalties from UpToDate. CAA has received royalties from UpToDate. All other authors have no conflicts to disclose.

Data Availability Statement

Datasets for the whole genome sequencing and RNA-seq are available at the National Center for Biotechnology Information (NCBI) under Bioproject Accession number PRJNA1025297.

344 **Online Methods**

345 *Bacterial strains, plasmids and growth conditions*

346 The bacterial strains and plasmids used in this work are listed in Supplemental Table 3. All
347 enterococcal strains were grown on brain heart infusion (BHI, Becton Dickinson) agar or in BHI
348 broth on rotating incubator at 37° C unless otherwise specified. The *Escherichia coli* strains
349 EC1000 and TG-1 were used for propagation of the plasmids pHOU1 and pAT392, respectively
350 and grown on Luria-Bertani (LB, Becton Dickinson) agar or in broth at 37° C supplemented with
351 25 µg/mL gentamicin (Sigma). Minimum inhibitory concentrations (MIC) were performed by
352 gradient diffusion test on Mueller-Hinton agar (MH, Becton Dickinson) for daptomycin, ampicillin,
353 vancomycin (Etest, bioMerieux), and bacitracin (MTS, Liofilchem). MICs for triclosan were
354 performed by broth microdilution in MH broth using two-fold serial dilutions of triclosan (range
355 0.125-128 µg/mL, Sigma). Bacterial growth curves were performed in a 96 well plate (Fisher)
356 with inoculation of approximately $5x10^5$ CFU/mL final concentration into a volume of 200 µL
357 BHI. Optical density at 600 nm was measured on a Synergy H1 plate reader (BioTek) over 24
358 hours at 15-minute intervals with 30 seconds of orbital shaking prior to each read.

359 *Genetic manipulation of strains*

360 Chromosomal deletions were generated using a derivative of OG1RF with the *E. faecalis* ATCC
361 4200 CRISPR1 *cas9* gene inserted in a neutral genomic insertion site to aid in genetic
362 manipulation.[28,29] A guide RNA for directed cleavage of the target sequence was provided in
363 trans in pCE under a constitutive pBac promoter. The pCE plasmid also contained a crossover
364 region containing approximately 800 bp up and downstream of the gene or region of interest.
365 PCR fragments were amplified from empty pCE, or purified enterococcal genomic DNA
366 templates, with approximately 20 bp complementary overhangs and assembled via Gibson
367 Assembly (Gibson Assembly Master Mix, New England Biolabs) by incubation in a thermal
368 cycler at 50° C for 1 hour. Primers used for each construct can be found in Supplemental Table
369 4. After assembly, the reaction was diluted 1:3 in nuclease free water and 6 µL was transformed
370 into chemically competent *E. coli* DH5α (High Efficiency, New England Biolabs). Transformants
371 were selected on LB agar with 15 µg/mL of chloramphenicol and screened with primers to
372 ensure correct plasmid and insert. Overnight cultures of *E. coli* with the construct of interest
373 were grown in LB broth with 15 µg/mL of chloramphenicol, plasmid was isolated (Wizard Plus
374 SV Miniprep DNA Purification System, Promega), and then electroporated into
375 electrocompetent *E. faecalis* OG117 or derivative as needed.[30] Transformants were selected on

376 BHI agar with 15 µg/mL of chloramphenicol. For constructs that could not be directly
377 electroporated, they were first electroporated into *E. faecalis* CK111, then filter mating with the
378 final strain was performed as previously described.[31] Transconjugants were selected on BHI
379 plus 15 µg/mL of chloramphenicol and 25 µg/mL fusidic acid. Colonies were then screened by
380 PCR to ensure the presence of the correct gene knock out or complementation. Curing of the
381 pCE plasmid was performed by streaking colonies on MM9-YEG plates containing p-chloro-
382 phenylalanine for counterselection. Colonies that grew on fusidic acid, but not chloramphenicol
383 or spectinomycin, were screened for presence of the plasmid and region of interest by PCR. All
384 constructs were verified by sanger sequencing over the entire crossover region, and whole
385 genome sequencing.

386 *RNA sequence analysis and qRT-PCR*

387 RNA-seq analysis was performed for the strains OG1RF, OG1RFΔ*madR*, and
388 OG1RF$madS_{A202E}$ as previously described.[10] Briefly, strains were grown overnight in tryptic soy
389 broth (TSB, Becton Dickinson) plus 50 mg/L of calcium chloride, then diluted into fresh TSB with
390 Ca^{2+} alone or with daptomycin at ½ of the MIC and grown to mid-exponential phase (OD_{600nm}
391 0.5-0.7) with agitation at 37° C. Cell pellets were harvested by centrifugation of 2 mL of mid-
392 exponential culture and stored at -80° C until extraction. Three independent biological replicates
393 were performed for each strain and treatment condition. Total RNA was obtained with the
394 Ribopure RNA purification kit (Ambion, Life Technologies) followed by DNase treatment, and
395 subsequent analysis for quality using Nanodrop (Thermo Scientific) and Bioanalyzer (Agilent).
396 Depletion of ribosomal RNA was performed using the Ribozero kit (Illumina). cDNA libraries
397 were prepared with the TrueSeq RNA Sample Preparation System v.2 (Illumina), and samples
398 were sequenced on an Illumina HiSeq2000. Reads were mapped using the OG1RF genome,
399 using the uninduced OG1RF as a reference for baseline expression. Reads per kilobase of
400 gene per million reads (RPKM) was calculated with EDGE-pro v1.3.1.[32] An adjusted p-value
401 threshold of $p < 0.01$ using the Benjamini-Hochberg procedure to control the false discovery
402 rate was used to identify the set of differentially expressed genes for each comparison with
403 DESeq2.[33]

404 Quantitative real-time PCR was performed as previously described.[10] Cells were grown
405 as above, in antibiotic induced and uninduced conditions, with either daptomycin or bacitracin-
406 zinc at ½ the respective MIC. Total RNA was isolated using the Pure Link RNA Isolation kit
407 (Invitrogen), genomic DNA was removed with the Turbo DNase kit (Ambion), and cDNA
408 synthesis was performed using SuperScript II Reverse Transcriptase (Invitrogen). Expression of

409 *madG*, *madL*, *madA*, and *dltA* were evaluated by qRT-PCR using SYBR Green in a CFX96
410 Touch Real-Time PCR Detection System (Bio-Rad). Expression level was quantified relative to
411 the control strain, OG1RF, without antibiotic exposure. Values were normalized to the
412 expression of *gyrB* as a housekeeping gene. Primers used for qRT-PCR are listed in
413 Supplemental Table 4. Fold-change was calculated using the Pfaffl method and primer
414 efficiency was determined for each reaction with the LinRegPCR program. Differences in gene
415 expression were determined using two-way ANOVA with Tukey's test for multiple comparisons,
416 with a p-value of < 0.05 (Graph Pad Prism). Each experiment was performed in biological and
417 technical triplicates.

418 *Antimicrobial peptide killing assays*

419 Antimicrobial peptide killing assays for LL-37 (50 µg/mL, Anaspec, Cat. #AS-61302), HBD3 (6
420 µg/mL, Anaspec, Cat. #AS-60741), and HNP-1 (10 µg/mL, Anaspec, Cat. #AS-60743) were
421 performed as previously described with modifications as follows.[34,35] All strains to be tested
422 were grown overnight in 5 mL of BHI broth on a rotary incubator at 37° C. Overnight cultures
423 were diluted 1:100 in 5 mL of fresh BHI broth and grown to mid-exponential phase (OD_{600nm} 0.5-
424 0.7). Strains were then adjusted to 0.5 McFarland (OD_{600nm} 0.08-0.1) in the respective assay
425 buffer: RPMI + 5% LB for LL-37 and HBD3 (HyClone RPMI 1640 without glutamine and without
426 phenol red, VWR), and 10 mM KH_2PO_4, pH 7.4 for HNP-1. Each respective McFarland standard
427 was further diluted in assay buffer to a final inoculum of $1x10^4$ CFU/mL and 5 µL of this
428 suspension was added to 45 µL of assay buffer with and without each antimicrobial peptide in
429 technical triplicate. Cells were then incubated for 2 hours at 37°C. After incubation, two serial
430 10-fold dilutions were made and 25 µL of each replicate was plated on fresh BHI agar plates.
431 Spots were allowed to dry, then incubated overnight at 37° C for colony counts. Percent survival
432 for each strain was calculated as CFU for peptide treated sample divided by the CFU for the
433 growth control sample times 100. Each assay was performed in three independent biological
434 replicates for each strain. Differences in mean survival were determined using one-way ANOVA
435 with Dunnet's multiple comparisons test, with a significance threshold of $p < 0.05$ (GraphPad
436 Prism).

437 *Cytochrome c assay*

438 Cell surface charge was determined by cytochrome c assay.[36] Overnight cultures were grown in
439 BHI broth to stationary phase, then pelleted by centrifugation, and resuspended in 1 mL of 20
440 mM MOPS buffer, pH 7.0 (Sigma). After resuspension, the suspension was transferred to a

441 microcentrifuge tube and washed twice with MOPS buffer. Washed cells were adjusted to a final
442 density of OD_{600nm} of 7.0, and 0.25 mg/mL of cytochrome c (bovine heart, Sigma) was added to
443 each sample and a cell free MOPS buffer control. Cytochrome c was allowed to bind for 15
444 minutes at 37° C with shaking, then cells were centrifuged at 14,000 relative centrifugal force for
445 5 minutes. An aliquot of 100 µL times 3 technical replicates was pipetted from the supernatant,
446 with care not to disturb the cell pellet, and transferred to a clear plastic 96-well plate.
447 Absorbance of each sample was read at 410 nm on a spectrophotometer (Synergy H1, BioTek).
448 The percentage bound cytochrome c was determined by calculating the difference from the
449 absorbance of the cytochrome c cell free control. Statistical comparison in the difference
450 between the mean level of binding was performed using one-way ANOVA with Dunnett's test for
451 multiple comparisons, with a significance threshold of $p < 0.05$ (GraphPad Prism).

452 *Membrane lipid extraction*

453 Lipids were extracted by the method of Bligh and Dyer, and as previously described.[37-39] Briefly,
454 bacteria were grown into mid-exponential phase or stationary phase, respectively, washed in 1x
455 phosphate buffered saline (PBS), then pelleted and dried in a centrifuge under vacuum. The
456 dried pellets were resuspended in 1 mL of sterile water (LC grade, Thermo Fisher Scientific),
457 then sonicated in an ice bath for 30 minutes to homogenize the sample. A 4 mL chilled solution
458 of chloroform and methanol (1:2 v/v, LC grade, Thermo Fisher Scientific) was added to each
459 tube and vortexed for 5 minutes. An additional 1 mL chilled chloroform and 1 mL chilled water
460 were added to each sample, vortexed for 1 minute, then centrifuged at 2,000 x *g* for 10 minutes
461 at 4° C. The organic layer was collected to a 10 mL glass centrifuge tube (Fisher Scientific) and
462 dried in a vacuum concentrator. The dried lipids were reconstituted in 500 µL of a 1:1 mixture of
463 chloroform and methanol and stored at -80° C until further use.

464 *Determination of membrane lipids by hydrophilic interaction chromatography-ion mobility-mass*
465 *spectrometry (HILIC-IM-MS)*

466 A 5 µL aliquot of each lipid extract was placed in LC vials, dried under nitrogen, and redissolved
467 in 100 µL of a 2:1 mixture of acetonitrile and methanol (LC grade, Thermo Fisher Scientific). The
468 lipids were separated on a Waters UPLC (Waters Corp., Milford, MA, USA) using a
469 Phenomenex Kinetex HILIC column (2.1x100 mm, 1.7 µm) at a temperature of 40° C and a flow
470 rate of 0.5 mL/minute.[40,41] A sample injection volume of 5 µL was used for each sample. The
471 solvent systems consisted of (A) 50% acetonitrile/50% water with 5 mM ammonium acetate
472 (Optima LC-MS grade, Thermo Fisher Scientific) and (B) 95% acetonitrile/5% water with 5 mM

473 ammonium acetate. The solvent gradient was 100% B 0-1 minutes, 90% B 4 minutes, 70% B 7-
474 8 minutes, 100% B 9-12 minutes.

475 Lipid analysis was performed on a Waters Synapt G2-XS platform. Samples separated
476 by the UPLC were injected via the electrospray ionization (ESI) source. ESI capillary voltages of
477 +2.0 were used for positive analyses and -2.0 kV for negative analyses. Additional ESI
478 conditions utilized were a sampling cone, 40 V; extraction cone, 80 V; source temperature, 150
479 °C; desolvation temperature, 500 °C; cone gas, 10 L/hr; desolvation gas, 1000 L/hr. Mass
480 calibration over *m/z* 50-1200 was performed with sodium formate. Calibration of ion mobility (IM)
481 measurements was performed as previously described.[42] IM separation was performed with a
482 traveling wave height of 40 V and velocity of 500 m/s. Data was acquired for *m/z* 50-1200 with a
483 1 sec scan time. Untargeted MS/MS (MS^E) was performed in the transfer region with a collision
484 energy ramp of 35-45 eV. Mass and drift time correction was performed post-acquisition using
485 the leucine enkephalin lockspray signal.

486 Data analysis was performed used the Progenesis QI software (Nonlinear Dynamics,
487 Milford, MA, USA) for alignment, peak detection, and normalization. A pooled quality control
488 sample was used as the alignment reference. All PC and PE lipid standards used for CCS
489 calibration were purchased from Avanti Polar Lipids.[43] The default "All Compounds" method of
490 normalization was used to correct for variation in the total ion current amongst samples. Lipid
491 identification was based on *m/z* (within 10 ppm mass accuracy), retention time, and CCS with
492 an in-house version of LipidPioneer, modified to contain the major lipid species observed in *E.*
493 *faecalis*, including DGs, DGDGs, PGs, CLs, and LysylPGs with fatty acyl compositions ranging
494 from 25:0 to 38:0 (total carbons : total degree unsaturation), and LiPydomics.[41,44,45]

495 Caenorhabditis elegans *infection model*

496 A *C. elegans* infection model was used to assess the impact of the loss of the MadR response
497 regulator on survival in wild type and *pmk-1* deficient nematodes.[46,47] Synchronized young adult
498 nematodes were infected with OG1RF, OG1RFΔ*madR*, or OG1RFΔ*madR* complemented with
499 *madR* in trans on pAT392 on BHI agar supplemented with 10 µg/mL of gentamicin.
500 Approximately 60-90 nematodes were transferred to a liquid media of 80% MW9 buffer and
501 20% BHI broth in 96 well plates. Plates were incubated at 25° C and evaluated daily for
502 nematode survival, which was assessed via movement on stimulation with a sterile platinum
503 wire probe. Survival curves were plotted using Kaplan-Meier log rank analysis, a difference in

504 median survival from three independent runs was considered significant with a p-value of <
505 0.05.

506 *Mouse peritonitis infection model*

507 A previously established mouse peritonitis model was used for this study.[48,49] The protocol was
508 approved by the University of Texas Health Science Center (UTHSC) Animal Welfare
509 Committee (AWC-19-0058). The lethal dose for 50% of animals (LD_{50}) for each strain was
510 calculated by the method of Reed and Muench.[50] Briefly, 4-6 week old female outbred ICR mice
511 (Envigo) weighing approximately 25 grams were inoculated (n=6 per strain) via intraperitoneal
512 injection of approximately $5x10^8$ CFU/mL in 50% sterile rat fecal extract. Mice were followed for
513 96 hours post infection, death was assessed approximately every 6 hours through the first 48
514 hours, then once daily through the end of the experiment. Differences in survival were
515 determined by Mantel-Cox (log-rank) test. At the time of death, spleen and heart were
516 aseptically excised. Spleens were added to pre-weighed bags, total tissue mass was calculated,
517 then the organs were homogenized with a paddle blender (Stomacher 80 Biomaster, Seward
518 Laboratory Systems). A total of 3 mL of sterile saline was added to each bag and mixed by
519 pipetting, then serial ten-fold dilutions were prepared and 50 µL of each dilution was plated in
520 triplicate onto fresh BHI agar plates. Plates were incubated overnight at 37° C, colonies were
521 enumerated, and normalized to the tissue mass. To assess for cardiac microlesions, hearts
522 were placed in formalin at the time of removal then processed by the UTHSC pathology core
523 laboratory.[18] The organs were embedded in paraffin, bisected, then sectioned longitudinally on a
524 microtome, with 32 sections per block. Every 4th section was stained with hematoxylin and eosin
525 (8 sections per animal). Microscopy was carried out on a Keyence BZ-X700 microscope. Each
526 lesion was imaged, the number of microlesions was determined for each section, and
527 differences between the mean number of microlesions per section for each strain were
528 calculated using one-way ANOVA with Tukey's test for multiple comparisons and a significance
529 threshold of $p < 0.05$. The area of each lesion was determined using FIJI software and
530 differences between the strains were determined using Kruskal-Wallis test with Dunn's test for
531 multiple comparisons.[51]

532

533

534

535 **Figures**

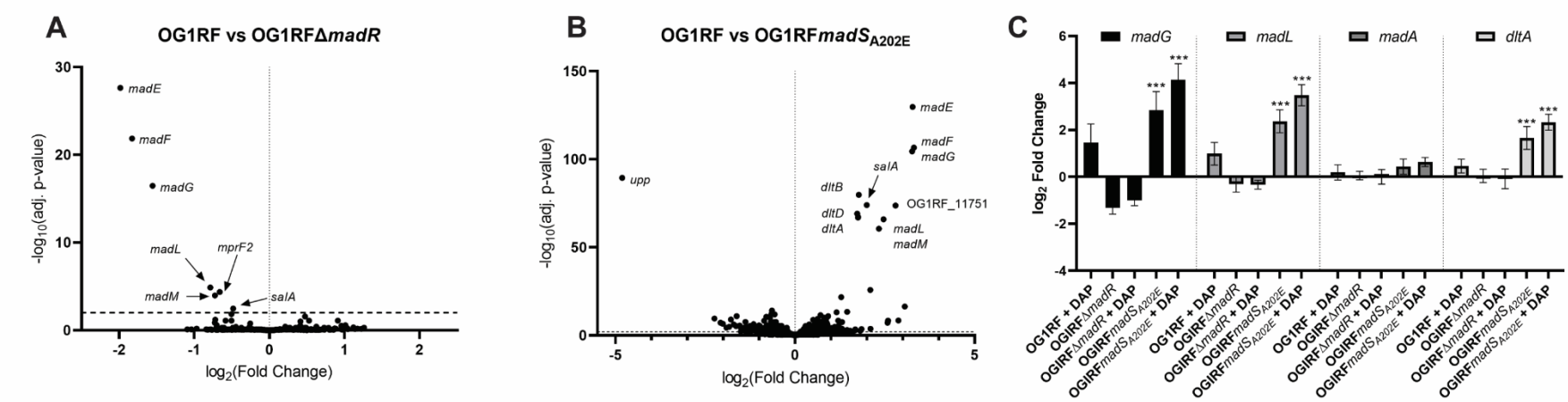

536

537 **Figure 1. Transcriptional profile of the MadRS regulon.** A) Gene expression by RNA sequence analysis of OG1RFΔ*madR* without
538 daptomycin exposure as compared to wild type OG1RF. The $\log_2$ fold change in gene expression is shown on the x-axis, and -
539 $\log_{10}$(adjusted p-value) is shown on the y-axis. Horizontal dotted line represents the significance cutoff of $p < 0.01$. B) Differentially
540 expressed genes in the OG1RF*madS*$_{A202E}$ as compared to OG1RF without daptomycin exposure. Select genes are labeled on the
541 plot, a full list of differentially expressed genes can be found in Supplemental Table 1. C) Quantitative reverse-transcriptase
542 polymerase chain reaction qRT-PCR) of representative genes of the MadRS system. Strains and antibiotic exposure conditions are
543 shown on the x-axis. Log_2 fold change in gene expression is shown on the y-axis. Error bars represent the standard deviation of
544 three independent biological runs performed in technical triplicate. Significant differences in gene expression were compared to
545 OG1RF without exposure to daptomycin. ***, $p < 0.001$.

546

547

548 **Figure 2.**

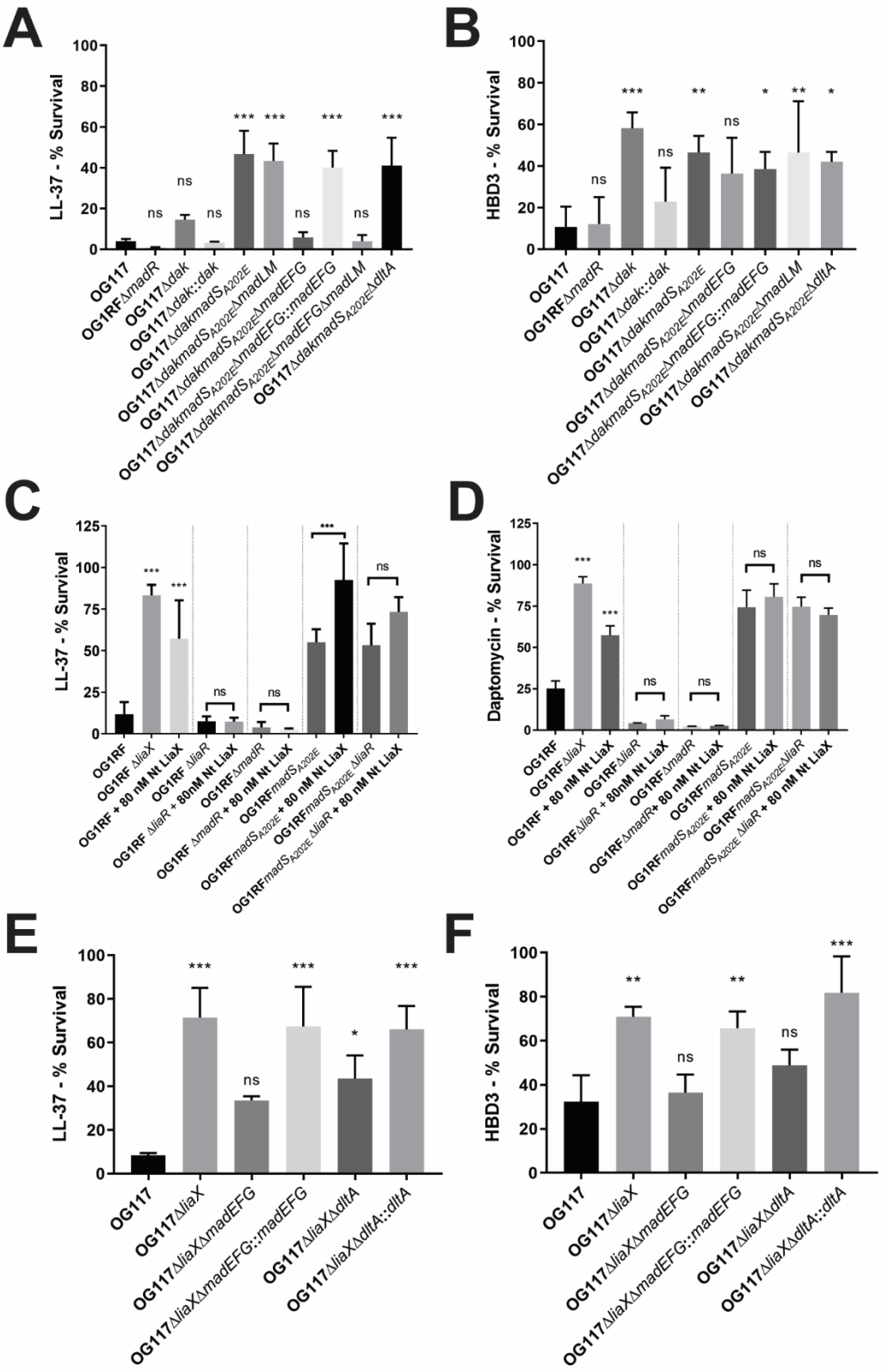

549

550 **Figure 2. MadRS mediates survival in the presence of antimicrobial peptides and**
551 **daptomycin independent of the LiaFSR system.** A) LL-37 killing assay (50 µg/mL of LL-37)
552 performed in OG117 background. Percent survival was calculated by dividing the colony
553 forming units per milliliter (CFU/mL) of the peptide free growth control with the CFU/mL of the
554 peptide treated samples. The OG117Δ*dakmadS*$_{A202E}$ strain (daptomycin resistant) showed a
555 significant increase in survival as compared to wild type OG117. Deletion of *madEFG*, but not
556 *madLM* alone or *dltA* led to increased killing by LL-37, and survival was restored on
557 complementation of *madEFG* in the native chromosomal location. B) HBD3 killing assay (6
558 µg/mL of HBD3) performed in the OG117 background. Deletion of *dak* was sufficient to increase
559 survival in the presence of HBD3. C) LL-37 and D) daptomycin (4 µg/mL) killing assay in the
560 OG1RF background, with and without the addition of N-terminal LiaX protein (Nt LiaX),
561 previously shown to protect *E. faecalis* from LL-37 mediated killing in a LiaFSR dependent
562 manner. Nt LiaX was unable to rescue a MadR knockout strain (pairwise comparisons are
563 shown as a bracket above strain pairs), and the presence of MadS$_{A202E}$ was able to confer
564 increased survival in the presence of both LL-37 and daptomycin in a strain lacking a functional
565 LiaFSR system (Δ*liaR*). E) LL-37 and F) HBD3 killing assay in the OG117Δ*liaX* background with
566 a constitutively active LiaFSR pathway. Deletion of *madEFG* decreased survival to a level that
567 was not statistically different from wild type. In the absence of membrane changes induced by
568 loss of *dak*, *madEFG* was also noted to be important for survival in the presence of HBD3.
569 Significant differences in survival between each strain and OG117 was determined by one-way
570 ANOVA. Error bars represent the standard deviation of three independent runs, performed in
571 biological triplicate on separate days. *, $p < 0.05$; **, $p < 0.01$; ***, $p < 0.001$; ns, not significant.

572

573

574

575

576

577

578

579 **Figure 3.**

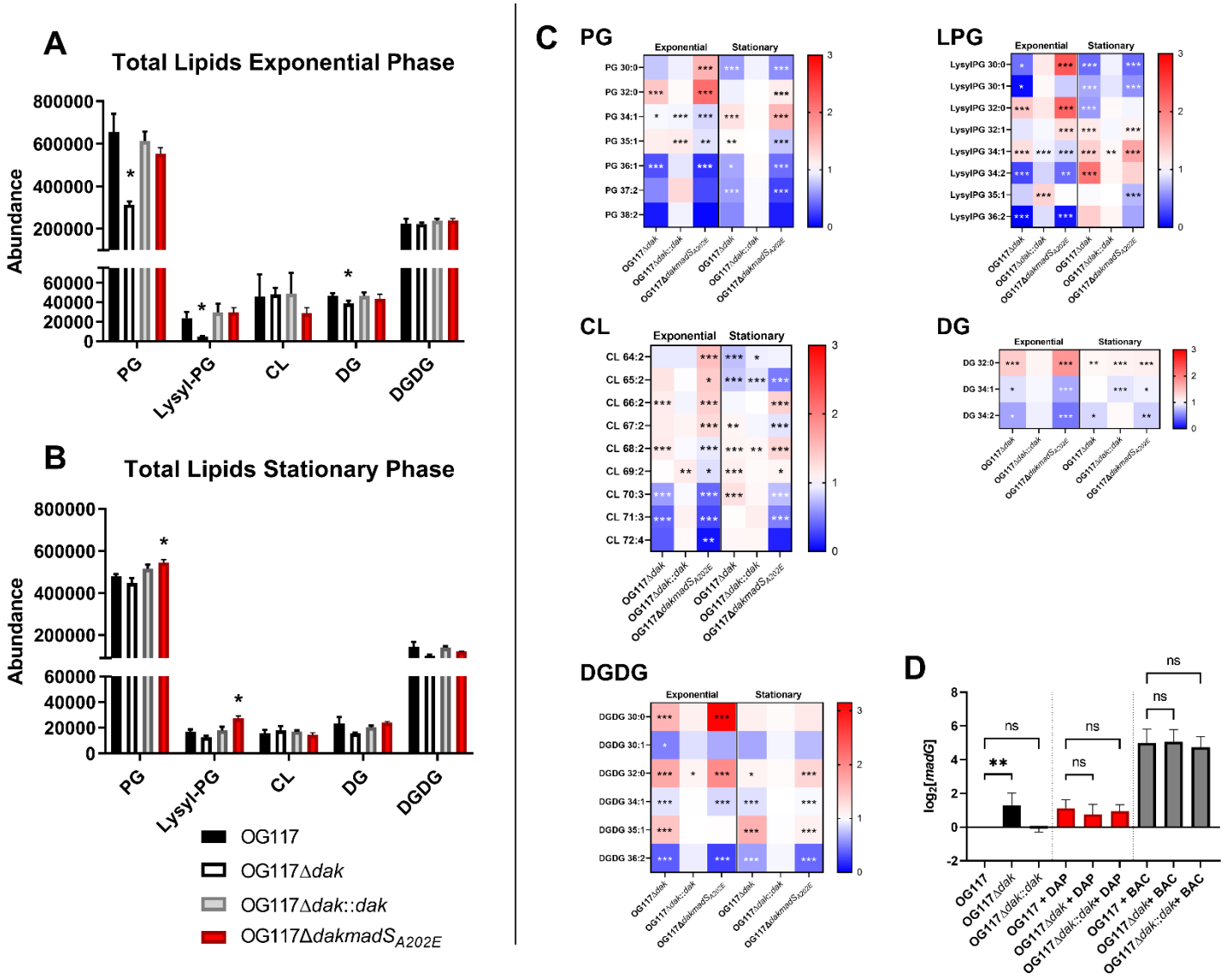
A
Total Lipids Exponential Phase
Abundance
800000
600000
400000
200000
60000
40000
20000
0
PG
Lysyl-PG
CL
DG
DGDG
B
Total Lipids Stationary Phase
OG117
OG117Δdak
OG117Δdak::dak
OG117ΔdakmadS$_{A202E}$
C
PG
LPG
CL
DG
DGDG
Exponential
Stationary
D
log$_2$[madG]
ns
**
OG117
OG117Δdak
OG117Δdak::dak
OG117 + DAP
OG117Δdak + DAP
OG117Δdak::dak+ DAP
OG117 + BAC
OG117Δdak+ BAC
OG117Δdak::dak+ BAC

580 **Figure 3. Deletion of *dak* is associated with changes in membrane fatty acyl composition**
581 **and alteration of *madG* expression.** Lipid analysis was carried out using Hydrophilic
582 interaction chromatography-ion mobility-mass spectrometry (HILIC-IM-MS). Total lipids in the A)
583 exponential growth and B) stationary phase were determined in the OG117 and *dak* deletion
584 strains. Relative abundance is listed on the y-axis, and each major enterococcal lipid species is
585 indicated on the x-axis. Significant differences in abundance of phosphatidylglycerol (PG),
586 Lysyl-PG, and diacylglycerol (DG) were seen in the *dak* deletion strain at exponential phase, but
587 not stationary phase. The OG117Δ*dakmadS*$_{A202E}$ strain developed a spontaneous mutation that
588 led to de-repression of the *fab* operon (see text). No differences were observed in this strain in
589 exponential phase, but there was a significant increase in PG and lysyl-PG at stationary phase.
590 C) Fatty acyl chain composition of PG, lysyl-PG (LPG), cardiolipin (CL), DG, and
591 digalactosyldiacylglycerols (DGDG) in exponential and stationary phase are shown as a heat
592 map based on relative change from wild type OG117, with red representing an increase and
593 blue representing a decrease in the relative proportion of each species. Carbon chain length
594 and number of unsaturated bonds are given (e.g., PG 34:1). Both strains with the *dak* deletion
595 showed a similar acyl chain profile, despite the constitutive activation of the FASII system in the
596 OG117Δ*dakmadS*$_{A202E}$ mutant. D) Expression of *madG* at exponential phase in the *dak* deletion
597 strains using qRT-PCR, without antibiotics (black bars), with daptomycin (DAP, red bars), and
598 with bacitracin (BAC, grey bars). In the absence of antibiotic stress, there was a significant 2.5-
599 fold increase in *madG* expression in the OG117Δ*dak* strain as compared to OG117. Under
600 daptomycin and bacitracin stress, there was no significant difference in *madG* expression
601 between the strains. *, $p < 0.05$; **, $p < 0.01$; ***, $p < 0.001$; ns, not significant.

602

603

604

605

606

607

608

609

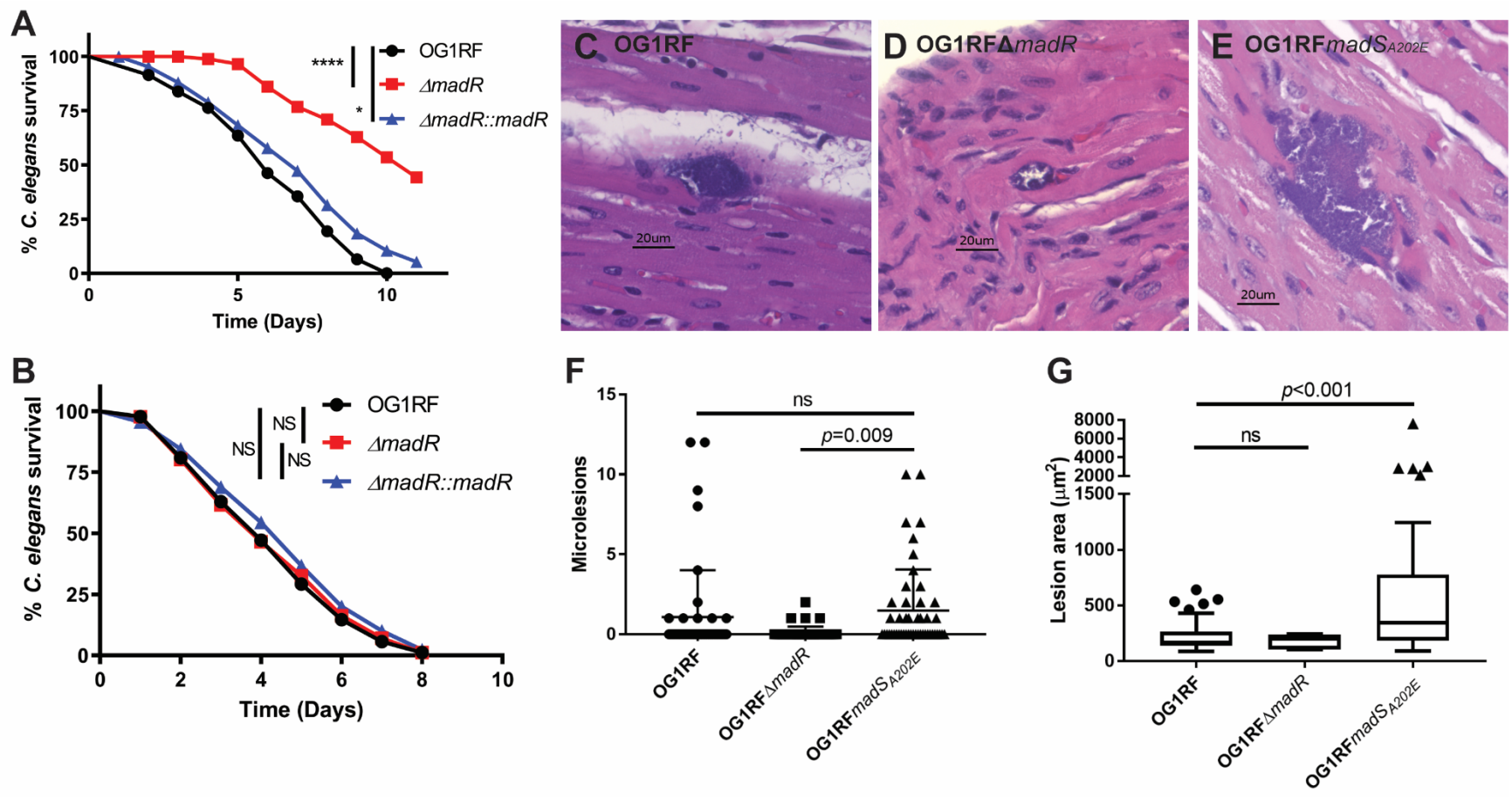

610

611 **Figure 4. The MadRS system protects *E. faecalis* from the host immune response *in vivo*.** Nematode survival in a C. elegans
612 model of infection with A) wild type nematodes and B) *pmk-1* knockouts deficient in antimicrobial peptide production. Nematodes
613 showed increased survival when infected with the OG1RFΔ*madR* strain as compared to the wild type OG1RF or when *madR* was
614 complemented in trans on a plasmid, however, no differences in survival were seen in the nematodes unable to produce AMPs. C-D)
615 Cardiac microlesions were assessed in a mouse model of peritonitis for the OG1RF, OG1RFΔ*madR*, and OG1RF*madS*$_{A202E}$ strains.
616 Murine hearts were formalin fixed and embedded in paraffin, bisected, then sectioned on a microtome. Representative micrographs

617 of hematoxylin and eosin stained sections are shown. F) Average number of cardiac microlesions per section. Eight sections were
618 evaluated per animal and 48 in total for each strain. Differences in the mean number of microlesions between each strain were
619 determined using one-way ANOVA. P-values are indicated for each comparison on the graph. G) Lesion area in μm^2 are given as
620 box and whisker plots of inner quartile range, with error bars plotted by the method of Tukey. Outliers are shown as individual data
621 points. Statistical differences between strains were assessed using the Kruskal-Wallis test. P-values are indicated for each
622 comparison on the graph. ns, not significant.

623

624

625

626

627

628

629

630

631

632

633

634

635

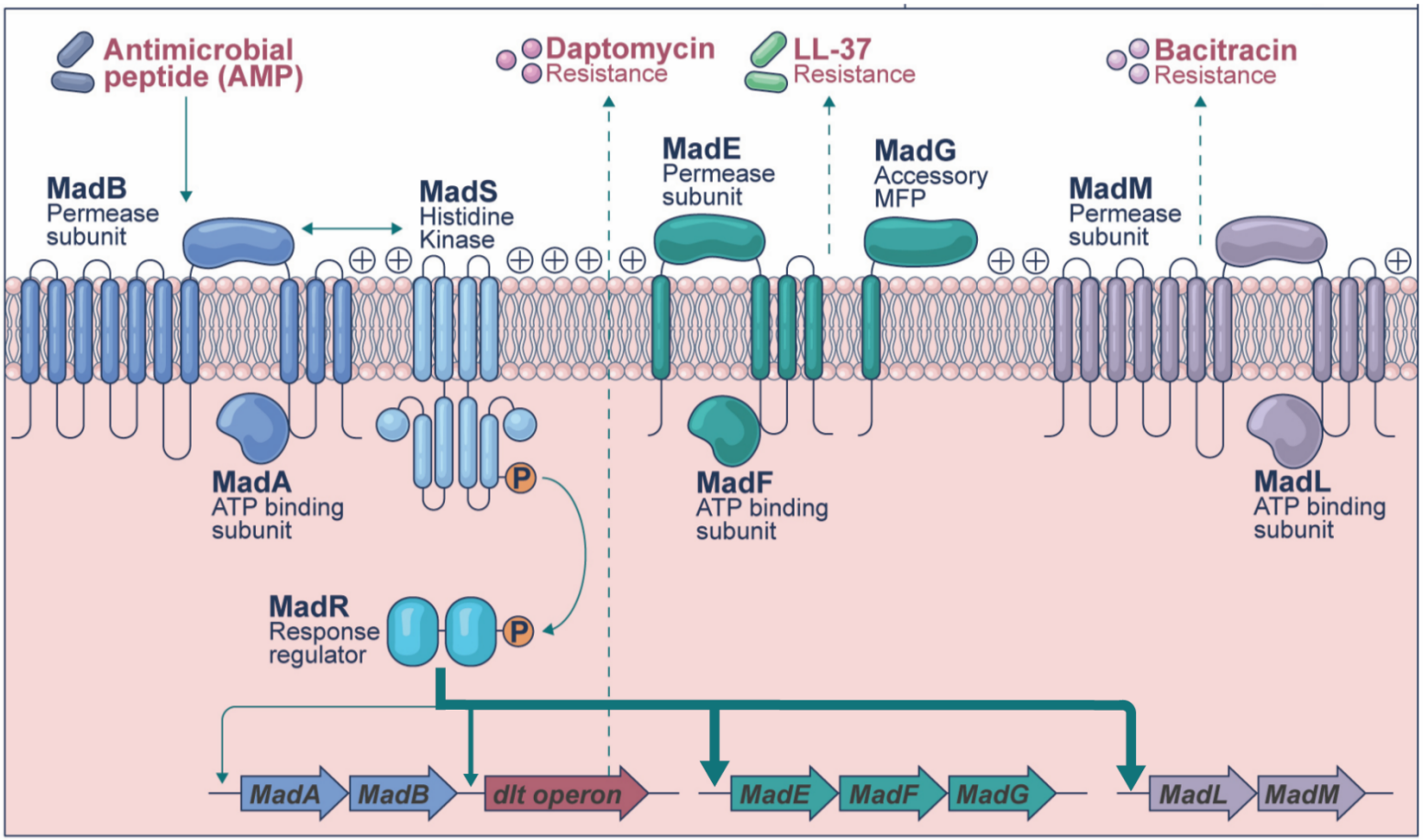

636

637 **Figure 5. Model for the function of the Membrane Antimicrobial Peptide Defense System.** The MadRS system controls a
638 network of effector proteins that provide a coordinated and specific defense against CAMPs and CAMP-like antibiotics. The MadS
639 sensor histidine kinase is activated by the flux-sensing mechanism of the constitutively expressed MadAB ATP-binding cassette
640 (ABC) transporter in the presence of AMPs. This leads to phosphorylation of the MadR response regulator and upregulation of the
641 genes encoding MadEFG, MadLM, and the *dlt* operon, as well as *mprF2* and the gene encoding a putative peptidoglycan hydrolase
642 SalA (not pictured). These targets each provide protection from their specific substrates including bacitracin (MadLM), LL-37 and

643 HBD3 (MadEFG), and daptomycin (DltABCD). After removal of CAMPs from the membrane by the ABC transporters, D-alanylation of
644 teichoic acids and lysylation of phosphotidylglycerol alters cell surface charge and prevents diffusion of these molecules back to the
645 cell membrane surface. Alterations of the cell membrane lipids (not pictured) via loss of function in *dak*, or other mechanisms, primes
646 expression of the MadRS system and may also directly interfere with CAMP binding.

647

648

649

650

651

652 **Table 1. Antimicrobial Minimum Inhibitory Concentrations (all values µg/mL).**

Strain	DAP	BAC	AMP	VAN
OG1RF	1.5	32	0.5	2
OG1RFΔ*liaR*	0.047	4	0.5	2
OG1RFΔ*madR*	0.38	12	0.5	3
OG1RF*madS*$_{A202E}$	6	96	1	3
OG117	1.5	32	0.75	3
OG117Δ*dak*	0.75	16	0.75	1.5
OG117Δ*dak::dak*	1.5	32	0.75	3
OG117Δ*dakmadS*$_{A202E}$	12	64	0.75	3
OG117Δ*dakmadS*$_{A202E}$Δ*madLM*	12	8	0.75	3
OG117Δ*dakmadS*$_{A202E}$Δ*madEFG*	12	64	0.75	3
OG117Δ*dakmadS*$_{A202E}$Δ*madEFG*::*madEFG*	8	64	1.5	3
OG117Δ*dakmadS*$_{A202E}$Δ*madEFG*Δ*madLM*	8	8	0.75	3
OG117Δ*dakmadS*$_{A202E}$Δ*dltA*	1.5	32	0.75	2
OG117Δ*dakmadS*$_{A202E}$Δ*dltA*::*dltA*	12	64	0.75	3
OG117Δ*liaX*	12	24	1	3
OG117Δ*liaX*Δ*madEFG*	12	24	1	3
OG117Δ*liaX*Δ*madEFG::madEFG*	16	24	0.75	3
OG117Δ*liaX*Δ*dltA*	2	32	1	2
OG117Δ*liaX*Δ*dltA::dltA*	12	24	0.75	3

653 AMP, ampicillin; BAC, bacitracin; DAP, daptomycin; VAN, vancomycin.

654

655

656

657

658

659

660

661

662

663

664 **References:**

665 1 Weiner-Lastinger, L. M. *et al.* Antimicrobial-resistant pathogens associated with adult
666 healthcare-associated infections: Summary of data reported to the National Healthcare
667 Safety Network, 2015-2017. *Infect Control Hosp Epidemiol* **41**, 1-18,
668 doi:10.1017/ice.2019.296 (2020).
669 2 Miller, W. R., Murray, B. E., Rice, L. B. & Arias, C. A. Resistance in Vancomycin-
670 Resistant Enterococci. *Infect Dis Clin North Am* **34**, 751-771,
671 doi:10.1016/j.idc.2020.08.004 (2020).
672 3 Dubin, K. & Pamer, E. G. Enterococci and Their Interactions with the Intestinal
673 Microbiome. *Microbiol Spectr* **5**, doi:10.1128/microbiolspec.BAD-0014-2016 (2014).
674 4 Miller, W. R., Bayer, A. S. & Arias, C. A. Mechanism of Action and Resistance to
675 Daptomycin in *Staphylococcus aureus* and Enterococci. *Cold Spring Harb Perspect Med*
676 **6**, doi:10.1101/cshperspect.a026997 (2016).
677 5 Grein, F. *et al.* Ca(2+)-Daptomycin targets cell wall biosynthesis by forming a tripartite
678 complex with undecaprenyl-coupled intermediates and membrane lipids. *Nat Commun*
679 **11**, 1455, doi:10.1038/s41467-020-15257-1 (2020).
680 6 Arias, C. A. *et al.* Genetic basis for in vivo daptomycin resistance in enterococci. *N Engl*
681 *J Med* **365**, 892-900, doi:10.1056/NEJMoa1011138 (2011).
682 7 Miller, W. R. *et al.* LiaR-independent pathways to daptomycin resistance in
683 Enterococcus faecalis reveal a multilayer defense against cell envelope antibiotics. *Mol*
684 *Microbiol* **111**, 811-824, doi:10.1111/mmi.14193 (2019).
685 8 Prater, A. G. *et al.* Environment Shapes the Accessible Daptomycin Resistance
686 Mechanisms in *Enterococcus faecium*. *Antimicrob Agents Chemother* **63**,
687 doi:10.1128/AAC.00790-19 (2019).
688 9 Tran, T. T. *et al.* Whole-genome analysis of a daptomycin-susceptible *Enterococcus*
689 *faecium* strain and its daptomycin-resistant variant arising during therapy. *Antimicrob*
690 *Agents Chemother* **57**, 261-268, doi:10.1128/AAC.01454-12 (2013).
691 10 Khan, A. *et al.* Antimicrobial sensing coupled with cell membrane remodeling mediates
692 antibiotic resistance and virulence in *Enterococcus faecalis*. *Proc Natl Acad Sci U S A*,
693 doi:10.1073/pnas.1916037116 (2019).
694 11 Prater, A. G. *et al.* Daptomycin Resistance in *Enterococcus faecium* Can Be Delayed by
695 Disruption of the LiaFSR Stress Response Pathway. *Antimicrob Agents Chemother* **65**,
696 doi:10.1128/AAC.01317-20 (2021).
697 12 Dintner, S. *et al.* Coevolution of ABC transporters and two-component regulatory
698 systems as resistance modules against antimicrobial peptides in Firmicutes Bacteria. *J*
699 *Bacteriol* **193**, 3851-3862, doi:10.1128/JB.05175-11 (2011).
700 13 Parsons, J. B. *et al.* Identification of a two-component fatty acid kinase responsible for
701 host fatty acid incorporation by *Staphylococcus aureus*. *Proc Natl Acad Sci U S A* **111**,
702 10532-10537, doi:10.1073/pnas.1408797111 (2014).
703 14 Harp, J. R. *et al.* Exogenous Fatty Acids Protect *Enterococcus faecalis* from
704 Daptomycin-Induced Membrane Stress Independently of the Response Regulator LiaR.
705 *Appl Environ Microbiol* **82**, 4410-4420, doi:10.1128/AEM.00933-16 (2016).
706 15 Popella, P. *et al.* VraH Is the Third Component of the *Staphylococcus aureus* VraDEH
707 System Involved in Gallidermin and Daptomycin Resistance and Pathogenicity.
708 *Antimicrob Agents Chemother* **60**, 2391-2401, doi:10.1128/AAC.02865-15 (2016).
709 16 Gebhard, S. *et al.* Identification and characterization of a bacitracin resistance network in
710 *Enterococcus faecalis*. *Antimicrob Agents Chemother* **58**, 1425-1433,
711 doi:10.1128/AAC.02111-13 (2014).

712 17 Zuo, G. *et al.* Structural insights into repression of the Pneumococcal fatty acid synthesis
713 pathway by repressor FabT and co-repressor acyl-ACP. *FEBS Lett* **593**, 2730-2741,
714 doi:10.1002/1873-3468.13534 (2019).
715 18 Brown, A. O. *et al.* Cardiac Microlesions Form During Severe Bacteremic *Enterococcus*
716 *faecalis* Infection. *J Infect Dis* **223**, 508-516, doi:10.1093/infdis/jiaa371 (2021).
717 19 DiPippo, A. J. *et al.* Daptomycin non-susceptible Enterococcus faecium in leukemia
718 patients: Role of prior daptomycin exposure. *J Infect* **74**, 243-247,
719 doi:10.1016/j.jinf.2016.11.004 (2017).
720 20 Ubeda, C. *et al.* Vancomycin-resistant Enterococcus domination of intestinal microbiota
721 is enabled by antibiotic treatment in mice and precedes bloodstream invasion in
722 humans. *J Clin Invest* **120**, 4332-4341, doi:10.1172/JCI43918 (2010).
723 21 Ramos, Y. *et al.* Remodeling of the Enterococcal Cell Envelope during Surface
724 Penetration Promotes Intrinsic Resistance to Stress. *mBio* **13**, e0229422,
725 doi:10.1128/mbio.02294-22 (2022).
726 22 Diagne, A. M. *et al.* Identification of a two-component regulatory system involved in
727 antimicrobial peptide resistance in *Streptococcus pneumoniae*. *PLoS Pathog* **18**,
728 e1010458, doi:10.1371/journal.ppat.1010458 (2022).
729 23 Yang, H. B. *et al.* Structure of a MacAB-like efflux pump from *Streptococcus*
730 *pneumoniae*. *Nat Commun* **9**, 196, doi:10.1038/s41467-017-02741-4 (2018).
731 24 Morris, S. M., Fritz, G., Rogers, T. & Gebhard, S. Novel regulatory logic in the antibiotic
732 resistance response of *Enterococcus faecalis* against cell envelope targeting antibiotics.
733 *bioRxiv*, doi:https://doi.org/10.1101/2022.11.16.516778 (2022).
734 25 George, N. L. & Orlando, B. J. Architecture of a complete Bce-type antimicrobial peptide
735 resistance module. *Nat Commun* **14**, 3896, doi:10.1038/s41467-023-39678-w (2023).
736 26 Ganz, T. Defensins: antimicrobial peptides of innate immunity. *Nat Rev Immunol* **3**, 710-
737 720, doi:10.1038/nri1180 (2003).
738 27 Hooper, L. V. & Macpherson, A. J. Immune adaptations that maintain homeostasis with
739 the intestinal microbiota. *Nat Rev Immunol* **10**, 159-169, doi:10.1038/nri2710 (2010).
740 28 Debroy, S. *et al.* Development of a genomic site for gene integration and expression in
741 Enterococcus faecalis. *J Microbiol Methods* **90**, 1-8, doi:10.1016/j.mimet.2012.04.011
742 (2012).
743 29 Price, V. J., Huo, W., Sharifi, A. & Palmer, K. L. CRISPR-Cas and Restriction-
744 Modification Act Additively against Conjugative Antibiotic Resistance Plasmid Transfer in
745 *Enterococcus faecalis*. *mSphere* **1**, doi:10.1128/mSphere.00064-16 (2016).
746 30 Hullahalli, K., Rodrigues, M., Nguyen, U. T. & Palmer, K. An Attenuated CRISPR-Cas
747 System in *Enterococcus faecalis* Permits DNA Acquisition. *mBio* **9**,
748 doi:10.1128/mBio.00414-18 (2018).
749 31 Panesso, D. *et al.* The hylEfm gene in pHylEfm of *Enterococcus faecium* is not required
750 in pathogenesis of murine peritonitis. *BMC Microbiol* **11**, 20, doi:10.1186/1471-2180-11-
751 20 (2011).
752 32 Magoc, T., Wood, D. & Salzberg, S. L. EDGE-pro: Estimated Degree of Gene
753 Expression in Prokaryotic Genomes. *Evol Bioinform Online* **9**, 127-136,
754 doi:10.4137/EBO.S11250 (2013).
755 33 Love, M. I., Huber, W. & Anders, S. Moderated estimation of fold change and dispersion
756 for RNA-seq data with DESeq2. *Genome Biol* **15**, 550, doi:10.1186/s13059-014-0550-8
757 (2014).
758 34 Reyes, J. *et al.* A *liaR* deletion restores susceptibility to daptomycin and antimicrobial
759 peptides in multidrug-resistant *Enterococcus faecalis*. *J Infect Dis* **211**, 1317-1325,
760 doi:10.1093/infdis/jiu602 (2015).
761 35 Jones, T. *et al.* Failures in clinical treatment of *Staphylococcus aureus* Infection with
762 daptomycin are associated with alterations in surface charge, membrane phospholipid

763 asymmetry, and drug binding. *Antimicrob Agents Chemother* **52**, 269-278,
764 doi:10.1128/AAC.00719-07 (2008).
765 36 Mishra, N. N. *et al.* Daptomycin resistance in enterococci is associated with distinct
766 alterations of cell membrane phospholipid content. *PLoS One* **7**, e43958,
767 doi:10.1371/journal.pone.0043958 (2012).
768 37 Garrett, T. A., Guan, Z. & Raetz, C. R. H. Analysis of ubiquinones, dolichols, and
769 dolichol diphosphate-oligosaccharides by liquid chromatography-electrospray ionization-
770 mass spectrometry. *Lipidomics and Bioactive Lipids: Mass-Spectrometry-Based Lipid*
771 *Analysis* **432**, 117-143, doi:10.1016/s0076-6879(07)32005-3 (2007).
772 38 Garrett, T. A., Kordestani, R. & Raetz, C. R. H. Quantification of cardiolipin by liquid
773 chromatography-electrospray ionization mass spectrometry. *Lipidomics and Bioactive*
774 *Lipids: Specialized Analytical Methods and Lipids in Disease* **433**, 213-230,
775 doi:10.1016/s0076-6879(07)33012-7 (2007).
776 39 Bligh, E. G. & Dyer, W. J. A Rapid Method of Total Lipid Extraction and Purification.
777 *Canadian Journal of Biochemistry and Physiology* **37**, 911-917 (1959).
778 40 Hines, K., Herron, J. & Xu, L. Assessment of Altered Lipid Homeostasis by HILIC-Ion
779 Mobility-Mass Spectrometry-Based Lipidomics. *J Lipid Res* **58**, 809-819,
780 doi:10.1194/jlr.D074724 (2017).
781 41 Hines, K. M. *et al.* Characterization of the Mechanisms of Daptomycin Resistance
782 among Gram-Positive Bacterial Pathogens by Multidimensional Lipidomics. *mSphere* **2**,
783 e00492-00417, doi:10.1128/mSphere.00492-17 (2017).
784 42 Hines, K. M., May, J. C., McLean, J. A. & Xu, L. Evaluation of Collision Cross Section
785 Calibrants for Structural Analysis of Lipids by Traveling Wave Ion Mobility-Mass
786 Spectrometry. *Anal Chem* **88**, 7329-7336, doi:10.1021/acs.analchem.6b01728 (2016).
787 43 Li, A., Hines, K. M. & Xu, L. in *Ion Mobility-Mass Spectrometry : Methods and Protocols*
788 (eds Giuseppe Paglia & Giuseppe Astarita) 119-132 (Springer US, 2020).
789 44 Ulmer, C. Z., Koelmel, J. P., Ragland, J. M., Garrett, T. J. & Bowden, J. A. LipidPioneer :
790 A Comprehensive User-Generated Exact Mass Template for Lipidomics. *J. Am. Soc.*
791 *Mass Spectrom.* **28**, 562-565, doi:10.1007/s13361-016-1579-6 (2017).
792 45 Ross, D. H., Cho, J. H., Zhang, R., Hines, K. M. & Xu, L. LiPydomics: A Python Package
793 for Comprehensive Prediction of Lipid Collision Cross Sections and Retention Times and
794 Analysis of Ion Mobility-Mass Spectrometry-Based Lipidomics Data. *Anal. Chem.*, DOI:
795 10.1021/acs.analchem.1020c02560. In Press., doi:10.1021/acs.analchem.0c02560
796 (2020).
797 46 Garsin, D. A. *et al.* A simple model host for identifying Gram-positive virulence factors.
798 *Proc Natl Acad Sci U S A* **98**, 10892-10897, doi:10.1073/pnas.191378698 (2001).
799 47 Kim, D. H. *et al.* A conserved p38 MAP kinase pathway in Caenorhabditis elegans innate
800 immunity. *Science* **297**, 623-626, doi:10.1126/science.1073759 (2002).
801 48 Arias, C. A., Singh, K. V., Panesso, D. & Murray, B. E. Evaluation of ceftobiprole
802 medocaril against *Enterococcus faecalis* in a mouse peritonitis model. *J Antimicrob*
803 *Chemother* **60**, 594-598, doi:10.1093/jac/dkm237 (2007).
804 49 Singh, K. V., Arias, C. A. & Murray, B. E. Efficacy of Tedizolid against Enterococci and
805 Staphylococci, Including cfr(+) Strains, in a Mouse Peritonitis Model. *Antimicrob Agents*
806 *Chemother* **63**, doi:10.1128/AAC.02627-18 (2019).
807 50 Reed LJ, M. H. A Simple Method of Estimating Fifty Per Cent Endpoints. *American*
808 *Journal of Epidemiology* **27**, 493-497,
809 doi:https://doi.org/10.1093/oxfordjournals.aje.a118408 (1938).
810 51 Schindelin, J. *et al.* Fiji: an open-source platform for biological-image analysis. *Nat*
811 *Methods* **9**, 676-682, doi:10.1038/nmeth.2019 (2012).

812